*IET Radar, Sonar & Navigation*

WILEY

The Institution of Engineering and Technology

ORIGINAL RESEARCH OPEN ACCESS

# Robust Low Rank 2D DoA Estimation and Adaptive Tracking for RIS-Assisted Vehicular Sensing Under Sparse Observations

Farheen Naaz[1] | Sung Won Kim[2]

[1]Department of Information and Communication Engineering, Yeungnam University, Gyeongsan, Republic of Korea | [2]School of Computer Science and Engineering, Yeungnam University, Gyeongsan, Republic of Korea

**Correspondence:** Sung Won Kim (swon@yu.ac.kr)

**Received:** 27 March 2026 | **Revised:** 24 April 2026 | **Accepted:** 12 May 2026

**Keywords:** direction-of-arrival estimation | intelligent networks | Kalman filters | wireless channels

## ABSTRACT

This paper proposes an adaptive framework for two-dimensional (2D) direction-of-arrival (DoA) estimation and tracking of two moving vehicles in reconfigurable intelligent surface (RIS)-assisted integrated sensing and communication (ISAC) systems. The considered scenario exploits RIS-reflected communication signals to sense and track two vehicles under sparse and intermittently activated RIS measurements. To mitigate the resulting degradation in spatial covariance estimation, a robust low-rank regularisation stage inspired by robust matrix completion (RMC) is applied prior to covariance estimation. Building on the regularised covariance information, a variable-forgetting and noise-adaptive recursive least squares tracker (VFN-RLS) is developed for robust DoA tracking, enabling rapid response to vehicle motion dynamics such as acceleration and turning manoeuvres. Simulation results under varying measurement sparsity, signal-to-noise ratio and impulsive-noise conditions show that the proposed framework significantly improves estimation accuracy over beamspace-only, tracking-only and partial-ablation baselines, whilst achieving competitive and often improved performance relative to Kalman and AF-RLS trackers. These results highlight the effectiveness of the proposed approach for low-complexity RIS-assisted vehicular sensing in dynamic urban transportation scenarios.

## 1 | Introduction

ISAC is emerging as a foundational paradigm for next-generation intelligent transportation systems (ITS), where wireless infrastructure is expected to simultaneously support high-rate data transmission and accurate environment sensing [1]. In vehicular networks, low-complexity estimation and tracking of the DoA of moving vehicles is critical for traffic monitoring, cooperative perception, collision avoidance and autonomous driving [2]. Achieving accurate and low-latency DoA tracking using communication-centric hardware therefore constitutes a key research objective for future V2X systems [3].

Unlike conventional radar or communication systems designed independently, ISAC enables sensing and communication functions to share spectrum, waveforms and hardware within a unified platform [4, 5], significantly improving spectral and energy efficiency whilst reducing hardware redundancy and deployment cost [6]. In vehicular scenarios, sensing can be performed either actively, using dedicated probing signals or passively, by extracting target parameters such as DoA, velocity and position from reflected communication signals [7]. This device-free sensing capability is particularly attractive for large-scale transportation systems, where deploying separate radar infrastructures is impractical [8, 9]. Nevertheless, the joint

operation of sensing and communication introduces new challenges in waveform design, beamforming and signal processing, especially under high mobility and stringent latency constraints [10].

RIS can further enhance ISAC-enabled sensing by providing programmable control over the wireless propagation environment [11]. An RIS consists of a large array of nearly passive reflecting elements whose electromagnetic response can be dynamically adjusted to manipulate the phase and in some cases the amplitude, of incident signals [12]. By intelligently reconfiguring these elements, RIS can establish virtual line-of-sight links, improve spatial diversity and enhance angular resolution without additional radio-frequency (RF) chains [13], making it particularly suitable for urban vehicular sensing scenarios where flexible coverage extension, low power consumption and hardware efficiency are paramount [14]. Recent studies further highlight the transformative role of RIS in vehicular networks, enabling coverage enhancement, interference mitigation and improved V2X connectivity [15].

Despite these benefits, practical RIS-assisted ISAC systems face significant challenges in dynamic vehicular environments [13]. Hardware and control constraints often require RIS elements to operate in a switching or partially activated manner, resulting in intermittent and incomplete sensing observations. Simultaneously, rapid vehicle motion induces fast time-varying DoA characteristics, making reliable estimation and low-complexity tracking considerably more difficult. Consequently, conventional estimation and tracking methods applied directly to such incomplete and noisy measurements suffer from substantial performance degradation, motivating the development of robust signal reconstruction and adaptive tracking frameworks capable of handling missing data, non-ideal propagation conditions and rapidly varying vehicle dynamics [16].

From a DoA estimation perspective, classical subspace-based methods such as MUSIC, ESPRIT, weighted subspace fitting (WSF) and maximum-likelihood (ML) estimators offer high resolution and strong theoretical guarantees. Recent advances have extended these foundations to practical array impairments such as mutual coupling [17]. RIS-aided passive localization using angle/time-of-arrival information in obstructed environments [18] and interference-aware RIS-assisted passive radar designs based on joint beamforming and phase-shift optimisation [19].

In RIS-assisted vehicular sensing, however, sparse RIS sampling, partial element activation and time-varying observation patterns frequently produce incomplete measurement matrices, rendering direct covariance estimation unreliable and causing significant degradation in DoA accuracy. Although compressed sensing and ANM can improve angular resolution, they incur high computational complexity and are better suited to static snapshot-based estimation than to real-time vehicular tracking. Matrix completion techniques offer a complementary alternative by exploiting the low-rank structure induced by a limited number of dominant targets; however, existing studies largely focus on signal reconstruction or one-shot estimation accuracy and the effect of regularised measurements on downstream DoA tracking remains largely unexplored.

From a tracking perspective, vehicular sensing is further complicated by nonstationary target motion, including abrupt changes in velocity and direction. Classical trackers such as the Kalman filter (KF) [20], extended Kalman filter (EKF) [21], unscented Kalman filter (UKF) [22] and recursive least squares (RLS)-based schemes [23] provide low-latency solutions, but fixed gain or fixed-forgetting-factor variants often fail to respond adequately to sudden manoeuvres. Although adaptive forgetting-factor RLS (AF-RLS) methods have been proposed [24], their integration with RIS-assisted sensing frameworks operating under sparse and intermittent observations remains limited.

Collectively, the existing literature reveals a clear gap in the development of a unified framework that jointly addresses sparse RIS observations, robust signal regularisation and dual-vehicle 2D DoA tracking under dynamic motion. This motivates an integrated processing pipeline combining robust measurement recovery with adaptive tracking, enabling reliable DoA estimation for two moving vehicles under incomplete measurements whilst maintaining low computational complexity. The present study focuses on a controlled two-vehicle scenario, enabling systematic assessment of sparse RIS observations, robust covariance stabilisation and adaptive tracking under heterogeneous motion patterns, including straight motion and turning manoeuvres.

It is noted that the proposed framework assumes two vehicles remain angularly distinguishable. In scenarios where multiple vehicles share nearly identical azimuth-elevation angles, additional diversity dimensions such as range, Doppler or frequency diversity may be required. Frequency-diversity-array (FDA)-based sensing frameworks have demonstrated potential for resolving co-angle targets through range-angle coupling [25] and incorporating such mechanisms into RIS-assisted sensing represents an important direction for future work. The framework further abstracts effects such as delay spread, Doppler spread, rich multipath and background clutter into effective noise terms, with the objective of evaluating the proposed signal processing and tracking pipeline under measurement sparsity and dynamic target motion rather than providing a comprehensive vehicular propagation model.

### 1.1 | Contributions

Motivated by the challenges of sparse RIS measurements and fast vehicular motion in ISAC systems, this paper proposes an adaptive RIS-assisted 2D DoA estimation and tracking framework for two moving vehicles. The main contributions are summarised as follows.

- We develop a RIS-assisted ISAC sensing system model for low-complexity 2D azimuth-elevation DoA estimation of two moving vehicles under intermittent RIS element activation and sparse observations
- To mitigate covariance estimation degradation caused by sparse and incomplete RIS measurements, we incorporate a robust low-rank regularisation preprocessing stage based on RMC and implemented via a Huber-loss ADMM formulation. Rather than recovering individual missing entries, the proposed approach seeks a robust low-rank representation

that preserves the dominant subspace and second-order statistics of the measurements, thereby stabilising beamspace spectrum extraction under sparse RIS activation.
- We propose a variable-forgetting and noise-adaptive recursive least squares (VFN-RLS) tracker for low-complexity 2D DoA tracking of two moving vehicles. The tracker adaptively adjusts its forgetting factor and process-noise inflation based on innovation statistics and motion dynamics, enabling rapid response to turning manoeuvres whilst maintaining robustness to measurement uncertainty.
- Simulation results under varying measurement sparsity, SNR and impulsive-noise conditions demonstrate that the proposed pipeline consistently improves estimation accuracy over beamspace-only, tracking-only and partial-ablation baselines, whilst achieving competitive and often improved performance relative to Kalman and AF-RLS trackers in the considered dual-vehicle scenario.

## 2 | System Model

Conventional DoA estimation relies on antenna arrays equipped with multiple RF chains, where spatial phase differences among received signals are exploited to infer target directions. Although effective, such multi-channel architectures incur high hardware cost, power consumption and system complexity, which restrict their scalability and practical deployment in large-scale sensing applications.

In this work, we consider a RIS-assisted sensing system for two moving vehicles, as illustrated in Figure 1. Two moving targets are present in the environment and their reflected signals are intercepted by a passive RIS and forwarded to a sensing receiver. Unlike traditional array-based systems, the receiver is equipped with a very limited number of RF chains, potentially as few as one, resulting in severely sparse spatial observations at each sensing snapshot [13].

The considered RIS-based sensing system exhibits the following key characteristics:

- **Passive RIS architecture:** The RIS consists of a large number of low-cost reflecting elements without RF chains or baseband processing and thus can only impose programmable phase shifts on the incident signals.
- **Discrete reflection control:** The RIS reflection coefficients are constrained to a finite set of discrete values, leading to phase quantisation effects and imperfect wavefront manipulation.
- **Sparse and intermittent measurements:** Due to RF-chain limitations and element switching, only a subset of RIS elements is observed at each instant, yielding incomplete measurement matrices.
- **Non-ideal noise conditions:** The low-cost hardware and dynamic propagation environment introduce non-Gaussian and impulsive distortions that deviate from idealised Gaussian noise assumptions.

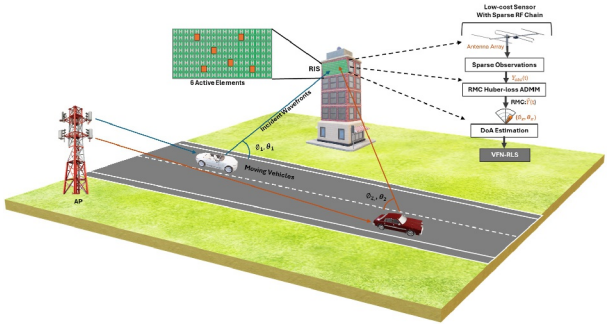


**FIGURE 1** | RIS-aided 2-D DoA estimation and target tracking.

Despite these limitations, the proposed system enables accurate low-complexity dual-target DoA estimation and tracking under sparse RIS observations. In the considered controlled sensing scenario, the two vehicles are assumed to be the dominant moving reflectors within the monitored region of interest. Static and miscellaneous background reflections from other urban objects are not explicitly modelled as separate semantic targets; instead, their aggregate effect is absorbed into the effective disturbance terms. Consequently, the present framework is designed to estimate and track dominant vehicle-related angular components rather than to guarantee perfect discrimination between vehicles and arbitrary clutter sources.

The sparse switching-based sensing model considered in this work is adopted to represent a low-complexity RIS sensing architecture in which only a limited number of sensing outputs are available at each sensing interval. Its purpose is not to suggest that sparse access is inherently superior to full element-wise observation, but rather to examine whether a large RIS aperture can still be exploited effectively when full sensing access is impractical. In this setting, switching provides a scalable means of sampling the RIS aperture over time whilst reducing sensing hardware complexity and acquisition overhead.

It is important to note that the considered RIS-assisted sensing configuration has a cascaded propagation structure: the communication signal first propagates from the transmitter to the vehicle and is then observed at the RIS via the vehicle-to-RIS reflected path. Accordingly, the departure angle associated with the transmitter-side illumination path and the arrival angle associated with the vehicle-to-RIS sensing path are, in general, distinct geometric quantities and are not assumed to be identical in this work. The proposed DoA estimation stage is formulated with respect to the signal impinging on the RIS aperture; therefore, the estimated angular parameters correspond to the receive-side arrival angles of the vehicle-reflected echoes.

### 2.1 | RIS Geometry and Received Signal Model

A two-dimensional planar RIS composed of $M_x$ rows and $M_y$ columns is considered, resulting in a total of $M = M_x M_y$ reflecting elements. Let $(m_x, m_y)$ denote the index of an RIS element, where $m_x \in \{0, \ldots, M_x - 1\}$ and $m_y \in \{0, \ldots, M_y - 1\}$. The RIS forms a large passive aperture that captures the spatial signatures of the impinging echo signals, whilst the sensing receiver is equipped with only a limited number of RF chains, leading to sparse observations across RIS elements. The transmitted communication signal illuminates the environment and is reflected by the targets. The resulting echo signals impinge on the RIS surface, forming the spatial aperture response.

Assume $K$ far-field narrowband targets whose reflected signals impinge on the RIS at sensing epoch $t$ with azimuth-elevation angle pairs $(\phi_k(t), \theta_k(t))$. These angles describe the receive-side direction of arrival of the vehicle-reflected echoes at the RIS aperture and do not imply equality with the transmitter-side illumination angles. Following a standard array-processing abstraction, the complex baseband signal induced at RIS element $(m_x, m_y)$ during the $\ell$-th time slot is modelled as

$$x_{m_x,m_y}(t,\ell) = \sum_{k=1}^{K} \alpha_k(t)\, \gamma_{m_x,m_y}\, a_{m_x,m_y}\big(\phi_k(t), \theta_k(t)\big)\, s_k(t,\ell), \quad (1)$$

where $\alpha_k(t)$ denotes the scattering coefficient of the $k$-th target, $\gamma_{m_x,m_y}$ represents the response coefficient of the $(m_x, m_y)$-th RIS element, capturing the local reflection and coupling characteristics of the RIS surface, $a_{m_x,m_y}(\phi,\theta)$ represents the RIS spatial response corresponding to direction $(\phi,\theta)$ and $s_k(t,\ell) \in \mathbb{C}$ denotes the unknown narrowband source symbol associated with the $k$-th target at time slot $\ell$. For notational simplicity, the target scattering coefficient $\alpha_k(t)$ and the element response $\gamma_{m_x,m_y}$ are absorbed into the effective source symbols $s_k(t,\ell)$ in the subsequent vector formulation. Although the signal model is presented in a general $K$-target form for notational convenience, the scope of this work is restricted to a controlled dual-target scenario, that is, $K = 2$.

For a uniform planar RIS, the steering coefficient can be expressed as

$$a_{m_x,m_y}(\phi,\theta) = e^{-j\frac{2\pi}{\lambda}\left(m_x d_x\, u_x(\phi,\theta) + m_y d_y\, u_y(\phi,\theta)\right)} \quad (2)$$

where $d_x$ and $d_y$ denote the inter-element spacings along the two RIS axes, $\lambda$ is the carrier wavelength and $\big(u_x(\phi,\theta), u_y(\phi,\theta)\big)$ are the direction cosines determined by the azimuth and elevation angles.

By stacking the element-wise responses into a vector $\mathbf{x}(t,\ell) \in \mathbb{C}^{M\times 1}$, the latent RIS aperture response can be written in compact form as

$$\mathbf{x}(t,\ell) = \sum_{k=1}^{K} \mathbf{a}\big(\phi_k(t), \theta_k(t)\big) s_k(t,\ell) = \mathbf{A}(t)\,\mathbf{s}(t,\ell), \quad (3)$$

where

$$\mathbf{A}(t) = \big[\mathbf{a}\big(\phi_1(t),\theta_1(t)\big), \ldots, \mathbf{a}\big(\phi_K(t),\theta_K(t)\big)\big] \in \mathbb{C}^{M\times K}, \quad (4)$$

$\mathbf{a}\big(\phi_k(t),\theta_k(t)\big) \in \mathbb{C}^{M\times 1}$ denotes the RIS steering vector of the $k$-th target and $\mathbf{s}(t,\ell) = [s_1(t,\ell), \ldots, s_K(t,\ell)]^{\mathsf{T}} \in \mathbb{C}^{K\times 1}$ collects the source symbols at slot $\ell$.

We consider a RIS-assisted sensing architecture in which a small number of active sensing outputs are attached to the RIS surface. Unlike conventional passive RIS designs that only apply programmable phase shifts to reflected signals, the proposed architecture enables sparse observation of RIS element responses through a switching-based sensing front-end. In this formulation, the steering matrix $\mathbf{A}(t)$ is constructed from the vehicle-to-RIS propagation geometry, since the arrival direction of the reflected echoes at the sensing side governs the RIS aperture response.

Let $\mathbf{x}(t,\ell) \in \mathbb{C}^M$ denote the latent RIS aperture response generated by the impinging signals, as described in Equations (2–4). Since the RIS does not provide direct baseband access to all $M$ elements, only a subset of RIS responses can be sensed at each slot. The available observation is therefore modelled as

$$\mathbf{y}(t,\ell) = \mathbf{S}_{\Omega_{t,\ell}}\,\mathbf{x}(t,\ell) + \mathbf{n}(t,\ell) + \mathbf{i}(t,\ell), \quad (5)$$

where $\Omega_{t,\ell} \subset \{1,\ldots,M\}$ denotes the active element set in slot $\ell$, $\mathbf{S}_{\Omega_{t,\ell}} \in \{0,1\}^{m_{\text{obs}}\times M}$ is the corresponding binary selection matrix and $m_{\text{obs}} = |\Omega_{t,\ell}| \ll M$. Here, $\mathbf{n}(t,\ell)$ models thermal noise and $\mathbf{i}(t,\ell)$ captures impulsive or non-Gaussian disturbances. Hence, the RIS sensing process is based on sparse element-sampled observations rather than full element-wise digital measurements.

Stacking the latent aperture responses over $L$ sensing slots gives

$$\mathbf{X}(t) = [\mathbf{x}(t,1), \ldots, \mathbf{x}(t,L)] \in \mathbb{C}^{M\times L}, \quad (6)$$

whilst the corresponding incomplete observation matrix is

$$\mathbf{Y}_{\text{obs}}(t) = \mathcal{P}_{\Omega_t}(\mathbf{X}(t) + \mathbf{N}(t) + \mathbf{I}(t)), \quad (7)$$

where $\mathcal{P}_{\Omega_t}(\cdot)$ denotes the slot-dependent sampling operator induced by the switching pattern $\Omega_t$ and $\mathbf{Y}_{\text{obs}}(t)$ contains missing entries corresponding to unobserved RIS elements. The aggregate effect of thermal noise, impulsive disturbances and hardware imperfections is represented by $\mathbf{N}(t)$ and $\mathbf{I}(t)$. The proposed sensing model assumes that the RIS switching pattern and the corresponding measurements within one sensing epoch are acquired over a sufficiently short time interval such that the vehicle motion can be regarded as locally quasi-static. Therefore, the target azimuth–elevation angles are assumed approximately constant during the formation of one sensing matrix, whereas their variation across successive epochs is handled by the tracking stage. Residual mismatch due to intra-epoch target motion is absorbed into the effective perturbation terms and is mitigated by the subsequent robust low-rank regularisation and adaptive tracking modules.

## 3 | Proposed Algorithm

The proposed framework addresses 2D DoA estimation and tracking of two moving vehicles under sparse RIS observations. Due to switching-based RIS acquisition, only a subset of RIS elements is observed at each sensing snapshot, which leads to incomplete spatial measurements and degrades conventional covariance-based DoA estimation. To improve robustness under such incomplete and impulsively corrupted observations, the proposed pipeline combines low-rank regularisation, beamspace DoA estimation and adaptive tracking, as illustrated in Figure 2.

### 3.1 | Algorithm Overview

The proposed algorithm consists of the following main stages.

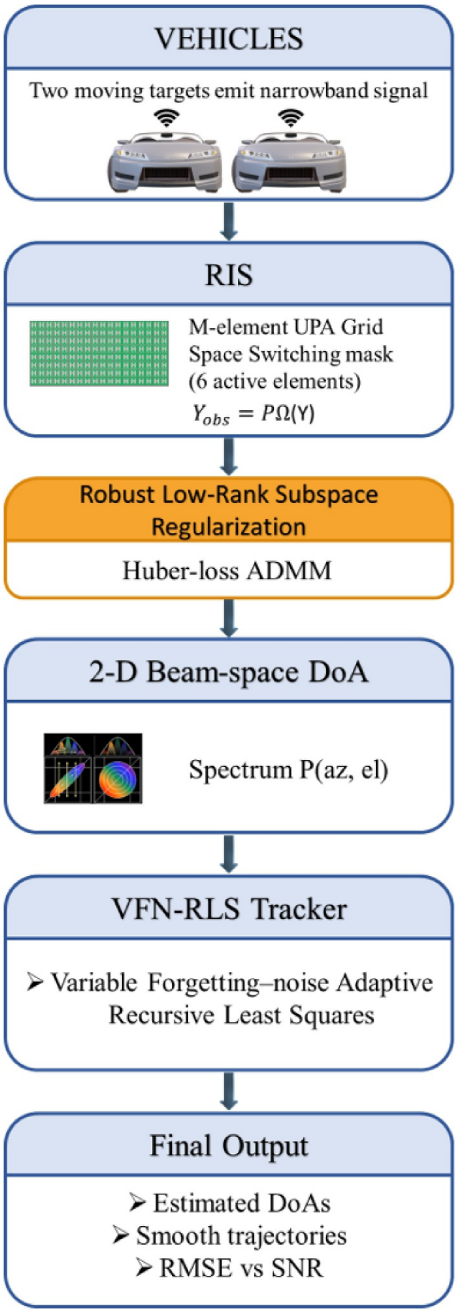


**FIGURE 2** | Flowchart of the proposed RIS-assisted 2D DoA estimation and tracking framework under sparse RIS observations.

#### 3.1.1 | *Sparse RIS Observation Model*

At each sensing epoch, RIS measurements are collected over multiple time slots using a switching-based acquisition mechanism. As a result, only a subset of RIS element–slot entries is observed, yielding a partially sampled measurement matrix [26–28].

#### 3.1.2 | *Low-Rank Subspace Stabilisation*

To mitigate the loss of spatial information caused by sparse RIS activation, a low-rank regularisation stage is applied prior to covariance formation. An ADMM-based formulation with Huber-type data fidelity is adopted to suppress impulsive disturbances whilst preserving the dominant signal subspace [29, 30]. Rather than targeting exact recovery of missing entries, this stage stabilises the covariance structure required for reliable beamspace DoA estimation [31].

#### 3.1.3 | *Beamspace-Based DoA Estimation*

The regularised measurement matrix is then used to estimate the instantaneous azimuth and elevation angles of the two vehicles. Beamspace spectrum processing is employed to extract the dominant angular peaks corresponding to the target directions [32].

#### 3.1.4 | *Adaptive DoA Tracking*

To track the time-varying DoAs of the two moving vehicles, a variable-forgetting and noise-adaptive recursive least squares tracker (VFN-RLS) is employed. By adjusting the forgetting factor according to innovation statistics and motion variation, the tracker improves robustness to abrupt manoeuvres and measurement fluctuations compared with fixed-forgetting-factor approaches [33].

### 3.2 | Robust Low-Rank Regularisation for Sparse RIS Measurements

Due to the switching-based acquisition imposed by the limited number of sensing outputs at the receiver, only a subset of RIS element responses can be accessed at each sensing epoch. Consequently, the observed measurement matrix $\mathbf{Y}_{\text{obs}}(t)$ contains missing entries corresponding to unobserved RIS elements. Such incomplete observations render direct covariance estimation unreliable and significantly degrade the performance of conventional subspace-based DoA estimation methods, particularly under low sampling ratios and dynamic propagation conditions. We emphasise that this setting is motivated by a hardware-constrained sparse-observation architecture, rather than by any claim that sparse acquisition is preferable to full observation. If all RIS element responses were directly available, covariance estimation would in general be more reliable. The proposed low-rank regularisation stage is therefore introduced specifically to improve robustness in the incomplete-observation regime considered in this paper. This challenge is further exacerbated in practical RIS-assisted sensing systems, where measurement noise may deviate from the ideal Gaussian assumption due to hardware nonlinearities, switching transients and intermittent interference.

The underlying noise-free RIS response matrix exhibits an intrinsic low-rank structure induced by the limited number of impinging sources. Specifically, from Equation (5), the noise-free signal matrix satisfies

$$\operatorname{rank}(\mathbf{X}(t)) \le K, \tag{8}$$

where $K \ll \min(M, L)$. This motivates low-rank regularisation for robust estimation under sparse observations.

Its effectiveness relies on three practical conditions: a small number of dominant targets, sufficiently informative RIS sampling across elements and slots and limited target motion within one sensing epoch. Hence, the proposed approach is intended

for sparse sensing regimes with approximate low-rank structure, rather than arbitrary missing-data scenarios.

Under extremely sparse sampling and impulsive corruption, exact entry-wise recovery is generally ill-posed. However, because the covariance in Equation (14) is computed from the regularised matrix, the recovered representation must still preserve the dominant second-order structure of the RIS observations. Therefore, the goal of the regularisation stage is not perfect reconstruction, but preservation of the dominant subspace and covariance-relevant structure required for reliable beamspace DoA estimation.

To this end, we adopt an RMC formulation that jointly enforces low-rank structure whilst mitigating the influence of impulsive noise. The problem is formulated as

$$\min_{\mathbf{X}} \|\mathbf{X}\|_* + \tau \sum_{(i,\ell)\in\Omega_t} \rho_\delta(Y_{i\ell}(t) - X_{i\ell}(t)), \tag{9}$$

where $\|\cdot\|_*$ denotes the nuclear norm promoting low-rank solutions [34], $\tau > 0$ controls the trade-off between data fidelity and rank regularisation, $\Omega_t$ denotes the index set of observed RIS elements at epoch $t$ and $\rho_\delta(\cdot)$ is the Huber loss function [35].

The Huber loss is defined as

$$\rho_\delta(e) = \begin{cases} \frac{1}{2}e^2, & |e| \le \delta, \\ \delta|e| - \frac{1}{2}\delta^2, & |e| > \delta, \end{cases} \tag{10}$$

which behaves quadratically for small residuals whilst growing linearly for large deviations, thereby reducing sensitivity to impulsive outliers caused by hardware impairments or abrupt propagation changes.

To efficiently solve Equation (9), an auxiliary variable $\mathbf{Z}$ is introduced, yielding the constrained formulation

$$\begin{aligned} \min_{\mathbf{X},\mathbf{Z}} \quad & \|\mathbf{Z}\|_* + \tau \sum_{(i,\ell)\in\Omega_t} \rho_\delta(Y_{i\ell}(t) - X_{i\ell}(t)) \\ \text{s.t.} \quad & \mathbf{X} = \mathbf{Z}. \end{aligned} \tag{11}$$

This problem is solved using the alternating direction method of multipliers (ADMM) [36]. The augmented Lagrangian is given by

$$\begin{aligned} \mathcal{L}(\mathbf{X},\mathbf{Z},\mathbf{\Lambda}) = {} & \|\mathbf{Z}\|_* \\ & + \tau \sum_{(i,\ell)\in\Omega_t} \rho_\delta(Y_{i\ell}(t) - X_{i\ell}(t)) \\ & + \frac{\mu}{2}\|\mathbf{X} - \mathbf{Z} + \mathbf{\Lambda}\|_F^2. \end{aligned} \tag{12}$$

where $\mathbf{\Lambda}$ is the scaled dual variable and $\mu > 0$ is the penalty parameter.

At each ADMM iteration, the $\mathbf{X}$-update corresponds to a Huber-regularised least-squares problem over the observed entries, whereas the $\mathbf{Z}$-update is obtained via singular value soft-thresholding [37],

$$\mathbf{Z}^{(n+1)} = \mathcal{D}_{1/\mu}\left(\mathbf{X}^{(n+1)} + \mathbf{\Lambda}^{(n)}\right), \tag{13}$$

where $\mathcal{D}_\alpha(\cdot)$ denotes the singular value thresholding operator as summarized in Algorithm 1. To reduce computational complexity and avoid overfitting noise, only the largest $r$ singular values are retained, with $r$ chosen proportional to the expected number of targets.

After convergence, the regularised matrix $\hat{\mathbf{X}}(t)$ provides a denoised low-rank representation of the RIS response, which is used to form the sample covariance

$$\hat{\mathbf{R}}(t) = \frac{1}{L}\hat{\mathbf{X}}(t)\hat{\mathbf{X}}^{\mathrm{H}}(t). \tag{14}$$

This covariance estimate serves as the input to the subsequent DoA estimation and dual-target tracking stages. Therefore, the regularised matrix $\mathbf{X}(t)$ must preserve the dominant spatial second-order structure of the RIS observations, even if exact entry-wise recovery is not achieved. In the proposed framework, RMC is employed as an optional initialisation-stage robustifier that accelerates covariance stabilisation under sparse and impulsively corrupted measurements, whereas asymptotic tracking performance is governed primarily by temporal aggregation.

**ALGORITHM 1** | Huber-ADMM Robust Low-Rank Regularisation (RMC)

**Input:** $\mathbf{Y}_{\mathrm{obs}}(t)$, $\Omega_t$, $\delta$, $\tau$, $\mu$, $r$, $N_{\max}$, $\epsilon$
**Output:** $\mathbf{X}_c(t)$
Initialise $\mathbf{X}^{(0)} = \mathbf{0}$, $\mathbf{Z}^{(0)} = \mathbf{0}$ and $\mathbf{\Lambda}^{(0)} = \mathbf{0}$.
**for** $n = 0$ to $N_{\max} - 1$ **do**
  Update $\mathbf{X}^{(n+1)}$
    Solve Huber-regularised least-squares over observed entries.
  Update $\mathbf{Z}^{(n+1)}$
    Apply truncated singular value thresholding (SVT) with rank $r$.
  Update dual variable
    $\mathbf{\Lambda}^{(n+1)} = \mathbf{\Lambda}^{(n)} + \mathbf{X}^{(n+1)} - \mathbf{Z}^{(n+1)}$.
  **if** $\frac{\|\mathbf{X}^{(n+1)} - \mathbf{Z}^{(n+1)}\|_F}{\|\mathbf{X}^{(n+1)}\|_F} < \epsilon$ **then break**.
**end for**
Return $\mathbf{X}_c(t) = \mathbf{X}^{(n+1)}$.

### 3.3 | Beamspace-Based 2D DoA Estimation

After obtaining the sample covariance matrix $\hat{\mathbf{R}}(t)$ in Equation (14), instantaneous azimuth–elevation DoA estimates are extracted using a beamspace spatial spectrum. Let $\mathbf{a}(\phi, \theta)$ denote the RIS steering vector corresponding to azimuth $\phi$ and elevation $\theta$. The spatial spectrum is computed as

$$P(\phi,\theta) = \mathbf{a}^H(\phi,\theta)\,\hat{\mathbf{R}}(t)\,\mathbf{a}(\phi,\theta). \tag{15}$$

The spatial spectrum in Equation (15) is evaluated over a discrete grid:

$$\phi \in \Phi = \left\{\phi_1, ..., \phi_{N_\phi}\right\}, \qquad \theta \in \Theta = \left\{\theta_1, ..., \theta_{N_\theta}\right\}. \tag{16}$$

Due to finite RIS aperture, limited temporal snapshots and measurement noise, the beamspace spectrum generally exhibits multiple local extrema rather than ideal impulse-like peaks. In multi-vehicle scenarios, each vehicle produces a dominant spectral lobe, whilst sidelobes and noise-induced fluctuations may also be present. Therefore, explicit peak detection is required to reliably extract physically meaningful DoA estimates and to separate multiple simultaneously present vehicles. This step converts the continuous spatial spectrum into discrete angular measurements suitable for subsequent temporal tracking.

Let $\mathbf{P} \in \mathbb{R}^{N_\phi \times N_\theta}$ denote the discretised two-dimensional spatial spectrum, whose $(i, j)$-th entry is given by

$$[\mathbf{P}]_{i,j} = P(\phi_i, \theta_j). \tag{17}$$

To estimate the DoAs of the two vehicles, the dominant spectral peaks are extracted from the beamspace spectrum $\mathbf{P}$. In the proposed framework, the azimuth domain is partitioned into two disjoint regions corresponding to the two targets, which exploits prior geometric knowledge of the controlled sensing scenario and helps prevent peak swapping between the two dominant angular lobes. This fixed split is adopted as a lightweight target-labelling mechanism under the assumption that the two vehicles remain sufficiently separable in azimuth during the observation interval. It is not intended to serve as a general multi-target data association method for arbitrary crossing or overtaking trajectories.

$$\left(\hat{\phi}_k, \hat{\theta}_k\right) = \arg \max_{\phi \in \Phi_k,\ \theta \in \Theta} P(\phi, \theta), \qquad k \in \{1, 2\}, \tag{18}$$

where $\Phi_1 = \{\phi < \phi_{\text{split}}\}$ and $\Phi_2 = \{\phi \geq \phi_{\text{split}}\}$ define the azimuthal regions for the two vehicles and $\phi_{\text{split}}$ is a predefined angular boundary determined by the RIS placement and road geometry.

The resulting DoA measurements are given by

$$\mathbf{z}_k(t) = \begin{bmatrix} \hat{\phi}_k(t) \\ \hat{\theta}_k(t) \end{bmatrix}, \qquad k \in \{1, 2\}, \tag{19}$$

which serve as inputs to the subsequent dual-target tracking stage.

### 3.4 | Bootstrap Initialisation and Target Association

At the initial sensing stage, a short observation window is used to collect instantaneous azimuth–elevation estimates from the beamspace spectrum over several consecutive sensing epochs. These preliminary DoA estimates are then grouped using a clustering procedure to identify two consistent angular patterns corresponding to the two vehicles. The resulting cluster centroids provide robust initial DoA estimates, which are used to initialise the trackers and establish the initial target association. This bootstrap initialisation improves tracker stability under sparse RIS observations by reducing sensitivity to noisy single-frame estimates.

Based on the bootstrap clustering results, the initial state of the $k$-th target tracker is initialised as

$$\mathbf{x}_k(0) = \begin{bmatrix} \phi_k^{(0)} \\ \dot{\phi}_k(0) \\ \theta_k^{(0)} \\ \dot{\theta}_k(0) \end{bmatrix} = \begin{bmatrix} \phi_k^{(0)} \\ 0 \\ \theta_k^{(0)} \\ 0 \end{bmatrix}, \tag{20}$$

where $\phi_k^{(0)}$ and $\theta_k^{(0)}$ denote the initial azimuth and elevation estimates of target $k$, obtained from the centroid of the corresponding bootstrap cluster formed from preliminary beamspace DoA estimates. The quantities $\dot{\phi}_k^{(0)}$ and $\dot{\theta}_k^{(0)}$ represent the initial azimuth and elevation angular rates, respectively and are set to zero because no prior motion information is assumed at the initialisation stage. Thus, the initial state vector contains both angular position and angular-rate components for each tracked target.

The proposed framework assumes a fixed number of targets and focuses on robust tracking under a controlled dual-target scenario with persistent angular separability. Consequently, the initialisation and target-labelling strategy based on the split boundary $\phi_{\text{split}}$ is suitable when the two dominant trajectories remain distinguishable in azimuth. More general dense-traffic data association scenarios involving lane changes, overtaking, intersecting trajectories or closely overlapping angular paths are outside the scope of the present study and would require dedicated probabilistic or assignment-based association mechanisms.

### 3.5 | Adaptive VFN-RLS Tracking Framework

To exploit temporal correlation in the estimated DoA measurements and enable smooth tracking of two moving vehicles, the instantaneous azimuth–elevation estimates obtained from the beamspace spectrum are processed using a VFN-RLS tracker.

Unlike conventional Kalman or fixed-forgetting RLS filters, the proposed VFN-RLS tracker dynamically adapts its memory depth and effective process noise based on the innovation statistics of the measurements, enabling rapid response to abrupt vehicle manoeuvres whilst maintaining stable tracking during steady motion.

For each vehicle $k$, the state vector is defined as

$$\mathbf{x}_k(t) = \left[\, \phi_k(t) \quad \dot{\phi}_k(t) \quad \theta_k(t) \quad \dot{\theta}_k(t) \,\right]^{\mathrm{T}}, \tag{21}$$

where $\phi_k(t)$ and $\theta_k(t)$ denote the azimuth and elevation angles, respectively and $\dot{\phi}_k(t)$ and $\dot{\theta}_k(t)$ represent their corresponding angular rates.

The tracker is initialised using the bootstrap DoA estimates obtained during the initial sensing stage, as described in Equation (20). Specifically, the initial azimuth and elevation angles are set to the bootstrap cluster centroids, whereas the angular rates are initialised to zero, providing a stable starting point for subsequent adaptive tracking. The proposed framework adopts a two-time-scale interpretation. Within each sensing epoch, the target directions are assumed approximately

stationary so that beamspace DoA estimation remains valid under RIS switching. Across sensing epochs, the angular variation caused by vehicle motion is captured by the adaptive state-space tracker.

Assuming a constant-velocity angular motion model, the state evolution equation is given by

$$\mathbf{x}(t) = \mathbf{F}\mathbf{x}(t-1) + \mathbf{w}(t), \tag{22}$$

where $\mathbf{w}(t) \sim \mathcal{N}(\mathbf{0}, \mathbf{Q}_t)$ denotes the process noise and the state transition matrix is defined as

$$\mathbf{F} = \begin{bmatrix} 1 & \Delta t & 0 & 0 \\ 0 & 1 & 0 & 0 \\ 0 & 0 & 1 & \Delta t \\ 0 & 0 & 0 & 1 \end{bmatrix}, \tag{23}$$

The sampling interval $\Delta t$ determines the temporal spacing between successive tracker updates and directly affects the validity of the constant-velocity angular motion model. When $\Delta t$ is sufficiently small, the azimuth and elevation of a moving vehicle can be approximated as evolving linearly over one update interval, making the model in Equation (23) a reasonable local approximation. However, for larger $\Delta t$, especially during abrupt manoeuvres such as sharp turns or U-turns, the true angular evolution may deviate significantly from this assumption, which can lead to larger innovations, transient lag and degraded tracking accuracy.

The complex RIS observations are first used to estimate the instantaneous DoA of each target using the proposed beamspace-based estimator. The resulting peak locations in the beamspace spectrum provide the angle estimates $\left(\hat{\phi}_k(t), \hat{\theta}_k(t)\right)$ for each vehicle $k$. These estimated angles are then used as the measurements for the tracking stage. Accordingly, the measurement model for the $k$-th vehicle is written as

$$\mathbf{z}_k(t) = \mathbf{H}\mathbf{x}_k(t) + \mathbf{v}_k(t), \tag{24}$$

where

$$\mathbf{z}_k(t) = \begin{bmatrix} \hat{\phi}_k(t) \\ \hat{\theta}_k(t) \end{bmatrix}$$

denotes the measured azimuth-elevation pair, $\mathbf{v}_k(t) \sim \mathcal{N}(\mathbf{0}, \mathbf{R})$ represents the measurement noise, and

$$\mathbf{H} = \begin{bmatrix} 1 & 0 & 0 & 0 \\ 0 & 0 & 1 & 0 \end{bmatrix}. \tag{25}$$

Because the RIS sensing process is based on intermittent element activation, the quality of the instantaneous DoA measurements may vary across sensing epochs depending on the active subset of RIS elements. As a result, the effective measurement disturbance may exhibit nonstationary behaviour and weak temporal dependence induced by the switching pattern. In the present framework, this effect is not modelled explicitly as a correlated noise process, but is absorbed into the aggregate measurement uncertainty handled by the adaptive tracking stage.

### 3.5.1 | *Innovation and Variance Tracking*

Given the predicted state $\hat{\mathbf{x}}^-(t)$ and covariance $\mathbf{P}^-(t)$, the innovation vector is computed as

$$\boldsymbol{\nu}_k(t) = \mathbf{z}_k(t) - \mathbf{H}\hat{\mathbf{x}}_k^-(t). \tag{26}$$

To capture time-varying measurement reliability, an exponentially smoothed innovation variance estimate is maintained according to

$$\hat{\sigma}^2_{\nu_k(t)}(t) = (1-\beta_e)\hat{\sigma}^2_{\nu_k(t)}(t-1) + \beta_e \|\boldsymbol{\nu}_k(t)\|^2, \tag{27}$$

where $\boldsymbol{\nu}_k(t) \in \mathbb{R}^{2\times 1}$ denotes the innovation vector at time index $t$, defined as the mismatch between the instantaneous DoA measurement and its predicted value and $\|\boldsymbol{\nu}_k(t)\|^2$ represents the squared innovation magnitude. The scalar $\hat{\sigma}^2_{\nu,k}(t)$ is an exponentially smoothed estimate of the innovation variance, which characterises the short-term reliability of the DoA measurements. For clarity, the main tracking variables are summarised as follows. The state vector of each target contains azimuth, azimuth rate, elevation and elevation rate. The matrix $\mathbf{P}^-(t)$ denotes the predicted state error covariance, whereas $\mathbf{P}(t)$ denotes the posterior covariance after measurement update. The matrix $\mathbf{Q}_0$ is the nominal process noise covariance and $\mathbf{Q}_t$ is its adaptively inflated version. The matrix $\mathbf{R}$ denotes the measurement noise covariance. In addition, $\eta_{\min}$ and $\eta_{\max}$ are the lower and upper bounds of the adaptive forgetting factor, $\beta_e$ is the smoothing parameter used for innovation-variance tracking, $\beta_Q$ controls process-noise inflation strength, $\theta_{\text{ref}}$ is the reference angular-rate threshold, $\delta$ is a small positive regularisation constant used in innovation normalisation and $\delta_\nu$ is the innovation clipping threshold used in the robust update stage.

In Equation (27), the smoothing factor $\beta_e \in (0,1)$ controls the memory depth of the estimator. A smaller $\beta_e$ yields a slowly varying variance estimate that is robust to outliers, whereas a larger $\beta_e$ enables faster adaptation to abrupt changes in the measurement statistics, such as those caused by rapid vehicle manoeuvres or transient multipath effects.

This adaptive innovation variance estimate serves as a normalisation reference for subsequent innovation-based adaptation, allowing the tracker to distinguish between nominal measurement noise and abnormal deviations. Consequently, the proposed formulation ensures stable yet responsive adjustment of the forgetting factor and process-noise inflation in highly dynamic vehicular scenarios.

A normalised innovation index is then defined as

$$\xi_k(t) = \frac{\|\boldsymbol{\nu}_k(t)\|^2}{\hat{\sigma}^2_{\nu,k}(t) + \delta}. \tag{28}$$

where $\delta > 0$ is a small regularisation constant. The corresponding bounded innovation excitation term is given by

$$f_1(t) = \frac{\xi(t)}{1 + \xi(t)}. \tag{29}$$

### 3.5.2 | *Motion-Aware Adaptation*

To incorporate target dynamics, an angular-rate proxy is computed from the predicted state as

$$\rho_k(t) = \sqrt{\dot{\hat{\phi}}_k^2(t) + \dot{\hat{\theta}}_k^2(t)}. \tag{30}$$

This quantity is mapped to a bounded motion excitation term

$$f_3(t) = \frac{\rho(t)}{\rho(t) + \theta_{\text{ref}} + \delta}, \tag{31}$$

where $\theta_{\text{ref}}$ denotes a reference angular-rate threshold controlling sensitivity to manoeuvring behaviour. Here, $f_1(t)$ denotes an innovation-driven excitation term that increases in response to large prediction errors between the estimated and observed DoAs, indicating potential measurement uncertainty or abrupt changes. In contrast, $f_3(t)$ captures motion-induced excitation derived from the estimated angular rates, reflecting target manoeuvring dynamics. The combination of these two terms allows the proposed tracker to adapt jointly to both measurement reliability and target motion characteristics.

### 3.5.3 | *Variable Forgetting Factor and Process Noise Inflation*

The innovation-driven and motion-driven terms are combined to form an adaptive excitation factor

$$\gamma(t) = \alpha_3 f_3(t) + \alpha_1 f_1(t) f_3(t), \tag{32}$$

where $\alpha_1$ and $\alpha_3$ are weighting coefficients. The excitation factor $\gamma(t)$ is bounded to the interval [0,1].

Based on $\gamma(t)$, the variable forgetting factor is defined as

$$\eta(t) = \eta_{\max} - (\eta_{\max} - \eta_{\min})\gamma(t). \tag{33}$$

where $\eta_{\min}$ and $\eta_{\max}$ denote the minimum and maximum forgetting factors, respectively.

Simultaneously, the process noise covariance is adaptively inflated according to

$$\mathbf{Q}_t = \kappa(t)\mathbf{Q}_0, \qquad \kappa(t) = 1 + \beta_Q \gamma(t), \tag{34}$$

where $\beta_Q$ controls the strength of process noise adaptation.

### 3.5.4 | *Robust Measurement Update*

To mitigate the influence of occasional outlying DoA estimates, Huber-type clipping is applied to the innovation:

$$\tilde{\boldsymbol{\nu}}(t) = \begin{cases} \boldsymbol{\nu}(t), & \|\boldsymbol{\nu}(t)\| \le \delta_\nu, \\ \delta_\nu \dfrac{\boldsymbol{\nu}(t)}{\|\boldsymbol{\nu}(t)\|}, & \text{otherwise}, \end{cases} \tag{35}$$

where $\delta_\nu$ denotes the clipping threshold.

Equations (32–34) describe the adaptive stage of the proposed VFN-RLS tracker. Specifically, $\mathbf{K}(t)$ denotes the tracker gain matrix, $\mathbf{P}^-(t)$ is the predicted state error covariance, $\mathbf{H}$ is the measurement matrix and $\mathbf{S}(t) = \mathbf{H}\mathbf{P}^-(t)\mathbf{H}^T + \mathbf{R}$ is the innovation covariance. The adaptive forgetting factor $\eta(t)$ scales the effective innovation weighting, allowing the tracker to balance responsiveness and stability.

$$\mathbf{K}(t) = \mathbf{P}^-(t)\mathbf{H}^{\mathrm{T}}\mathbf{S}^{-1}(t), \tag{36}$$

where $\mathbf{P}^-(t)$ denotes the predicted state error covariance, $\mathbf{H}$ is the measurement matrix and $\mathbf{S}(t)$ is the innovation covariance. The adaptive forgetting factor $\eta(t)$ directly scales the innovation covariance, enabling the tracker to dynamically balance memory retention and responsiveness. A smaller $\eta(t)$ increases the effective gain, allowing rapid adaptation during sharp target manoeuvres, whereas larger values promote stability under steady motion. The complex RIS snapshots are used solely for instantaneous DoA estimation, whereas the proposed tracker operates on the resulting angle estimates obtained from the spatial spectrum.

Using the gain in Equation (36), the state estimate is updated as

$$\hat{\mathbf{x}}(t) = \hat{\mathbf{x}}^-(t) + \mathbf{K}(t)\tilde{\boldsymbol{\nu}}(t), \tag{37}$$

where $\hat{\mathbf{x}}^-(t)$ is the predicted state vector and $\tilde{\boldsymbol{\nu}}(t)$ denotes the robustified innovation obtained after Huber-based clipping. This operation corrects the predicted azimuth and elevation states based on reliable measurement information whilst suppressing the influence of large innovation outliers.

Finally, the posterior error covariance matrix is updated according to

$$\mathbf{P}(t) = (\mathbf{I} - \mathbf{K}(t)\mathbf{H})\mathbf{P}^-(t), \tag{38}$$

where $\mathbf{S}(t) = \mathbf{H}\mathbf{P}^-(t)\mathbf{H}^{\mathrm{T}} + \mathbf{R}$ is the innovation covariance. The detailed procedure of the proposed tracking stage is summarised in Algorithm 2.

**ALGORITHM 2** | Beamspace 2D DoA Estimation and VFN–RLS Tracking for Two Moving Vehicles

**Input:** Regularised covariance matrix $\hat{\mathbf{R}}(t)$, angle grids $\Phi, \Theta$, split angle $\phi_{\text{split}}$ and initialisation parameters.

**Output:** Tracked DoAs $\left\{\left(\hat{\phi}_k(t), \hat{\theta}_k(t)\right)\right\}_{k=1}^{2}$ for each time instant $t$.

Initialise $\hat{\mathbf{x}}_k(0)$, $\mathbf{P}_k(0) = \Delta^{-1}\mathbf{I}$ and $\hat{\sigma}^2_{\nu,k}(0)$ for $k = 1, 2$.

**for** $t = 1$ to $T$ **do**

Compute beamspace spectrum

$$P(\phi, \theta) = \mathbf{a}^{\mathrm{H}}(\phi, \theta)\hat{\mathbf{R}}(t)\mathbf{a}(\phi, \theta)$$

Extract peaks

$$\left(\hat{\phi}_k, \hat{\theta}_k\right) = \arg\max_{\phi \in \Phi_k, \theta \in \Theta} P(\phi, \theta), \quad k = 1, 2$$

Prediction

$$\hat{\mathbf{x}}_k{}^-(t) = \mathbf{F}\hat{\mathbf{x}}_k(t-1)$$

$$\mathbf{P}_k{}^-(t) = \mathbf{F}\mathbf{P}_k(t-1)\mathbf{F}^{\mathrm{T}} + \kappa_k(t-1)\mathbf{Q}_0$$

Innovation

$$\boldsymbol{\nu}_k(t) = \mathbf{z}_k(t) - \mathbf{H}\hat{\mathbf{x}}_k{}^-(t)$$

Variance update

$$\hat{\sigma}^2_{\nu,k}(t) = (1 - \beta_e)\hat{\sigma}^2_{\nu,k}(t-1) + \beta_e \|\boldsymbol{\nu}_k(t)\|^2$$

Compute adaptive parameters $\eta_k(t)$ and $\kappa_k(t)$ based on innovation and motion metrics.

Gain and state update

$$\mathbf{K}_k(t) = \mathbf{P}_k{}^{-}(t)\mathbf{H}^{\top}\big(\eta_k(t)\mathbf{S}_k(t)\big)^{-1}$$

$$\hat{\mathbf{x}}_k(t) = \hat{\mathbf{x}}_k{}^{-}(t) + \mathbf{K}_k(t)\tilde{\boldsymbol{\nu}}_k(t)$$

**end for**

## 4 | Simulation Results

This section presents numerical simulation results to evaluate the accuracy, robustness and computational efficiency of the proposed RIS-assisted 2D DoA estimation and tracking framework. The framework is assessed from two complementary perspectives. First, the contribution of each component is quantified through an ablation study. Second, the robustness and dynamic behaviour of the proposed method are analysed under impulsive noise and manoeuvring conditions. The detailed simulation parameters are summarised in Table 1.

We consider a RIS-assisted vehicular sensing scenario in an urban environment, where a base station (BS) exploits RIS-reflected signals to estimate and track the two-dimensional directions of arrival (DoAs) of two moving vehicles. The RIS is mounted on a building façade at $H_{\mathrm{RIS}} = 15$ m and comprises a $10 \times 10 = 100$-element uniform planar array. Due to hardware and energy constraints, only $M_{\mathrm{obs}} = 6$ elements ($\approx 6\%$) are activated per sensing snapshot via a switching-based acquisition mechanism.

A straight road segment is situated at $Y_{\mathrm{road}} = 60$ m from the RIS, along which two vehicles ($K = 2$) move with distinct initial positions and velocities. Vehicle 1 starts at $X_{1,0} = -25$ m with $V_1 = 15$ m/s and executes a U-turn manoeuvre after a certain time instant, whereas Vehicle 2 starts at $X_{2,0} = 30$ m with $V_2 = 10$ m/s along a straight trajectory. The resulting motion induces distinct time-varying azimuth and elevation angle profiles at the RIS, as illustrated in Figure 3. The azimuth and elevation search ranges are set to $[-60°, 60°]$ and $[-20°, 20°]$, respectively and the SNR is varied over $\{-5, 0, 5, 10, 15, 20\}$ dB to assess robustness under diverse noise conditions. The proposed framework integrates robust low-rank regularisation with adaptive DoA tracking to enable reliable estimation under sparse RIS activation and dynamic vehicular motion.

**TABLE 1** | Simulation parameters.

| Parameter | Description | Value |
|---|---|---|
| $f_c$ | Carrier frequency | 28 GHz |
| $\lambda$ | Wavelength | $c/f_c$ |
| $d$ | Inter-element spacing | $0.5\lambda$ |
| $M_x \times M_y$ | RIS array size | $10 \times 10$ |
| $K$ | Number of targets | 2 |
| $L$ | Snapshots per sensing epoch | 32 |
| $T_s$ | Tracking update interval | 0.05 s |
| $\tau$ | Low-rank regularisation weight | $10^{-3}$ |
| $\delta$ | Huber loss parameter | 1 |
| $\mu$ | ADMM penalty parameter | 1 |
| $r$ | Rank truncation parameter | 4 |

Figure 4 illustrates the azimuth tracking performance of the proposed framework. Target 1 executes a U-turn manoeuvre, inducing an abrupt directional change, whereas Target 2 follows a smooth straight trajectory. The proposed method successfully tracks both targets under sparse RIS observations.

A transient deviation is observed for Target 1 during the turning phase, arising from the combined effects of rapid motion dynamics, a momentary mismatch between the constant-velocity angular model and the true U-turn trajectory and the reactive nature of the adaptive process-noise inflation, which is triggered only after the manoeuvre onset. Despite this short-lived deviation, the VFN-RLS tracker rapidly re-converges to the true

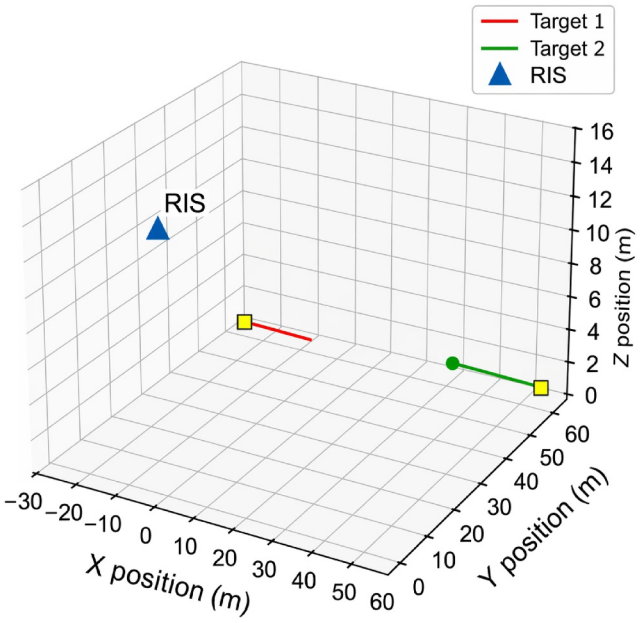


**FIGURE 3** | 3D ground-truth vehicle trajectories in RIS-assisted scenario.

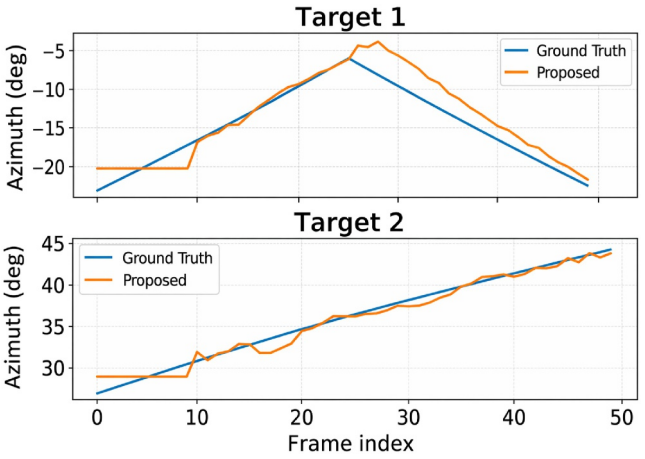


**FIGURE 4** | Azimuth DoA tracking performance for two moving targets.

trajectory, confirming robust recovery under nonstationary target motion and demonstrating a practical balance between tracker responsiveness and stability.

Overall, the results indicate that the proposed framework provides a practical balance between responsiveness and robustness under nonstationary target motion.

Figure 5a,b present the azimuth RMSE versus SNR for Target 1 and Target 2, respectively, comparing the Kalman filter, AF-RLS and the proposed RMC + VFN-RLS algorithm. Although all methods benefit from increasing SNR, the proposed algorithm achieves the lowest or near-lowest RMSE across the entire SNR range. At a lower SNR, the Kalman filter and AF-RLS exhibit substantial degradation due to limited robustness against noise and incomplete measurements, whereas the proposed method maintains significantly lower RMSE, confirming superior noise resilience and tracking stability.

Figure 5c,d further examine Target 1 performance before and after the U-turn manoeuvre, respectively. Before the manoeuvre, where the target follows a smooth trajectory, the proposed algorithm already achieves the lowest estimation error under nominal motion conditions. After the U-turn, the performance gap widens considerably: the Kalman filter and AF-RLS struggle to adapt to the abrupt directional change, incurring a pronounced RMSE increase, whereas the proposed method rapidly re-converges and preserves low error levels. These results confirm that combining robust low-rank regularisation with the adaptive VFN-RLS tracker substantially enhances tracking capability under both nominal and highly dynamic sensing conditions.

Figure 6a,b present the azimuth RMSE versus impulsive-noise probability $p_{\text{imp}}$ for Target 1 and Target 2, respectively. Both targets exhibit a general degradation in estimation accuracy with increasing impulsive disturbance. For Target 1, minor non-monotonic fluctuations are observed in Figure 6a, attributable to the interplay between sparse RIS observations and the challenging U-turn dynamics. Target 2, following a smoother trajectory, yields the more regular upward RMSE trend seen in Figure 6b. Across the entire $p_{\text{imp}}$ range, the proposed method consistently achieves lower RMSE than both the Kalman filter and AF-RLS, demonstrating superior robustness against impulsive noise.

Figure 7 illustrates the temporal evolution of the instantaneous azimuth tracking error, defined as $|\theta_{\text{est}} - \theta_{\text{true}}|$, for Target 1 (top) and Target 2 (bottom). Since all RMC-based trackers yield nearly identical azimuth error profiles, a single representative curve is shown for clarity.

For Target 1, the RAW + VFN method exhibits large and persistent errors, reflecting poor robustness to sparse and noisy measurements, whereas SVT + VFN provides only partial improvement with noticeable fluctuations. The proposed RMC-based tracker rapidly converges after a brief transient and maintains consistently low error throughout the observation interval. Target 2 follows the same trend: RAW + VFN

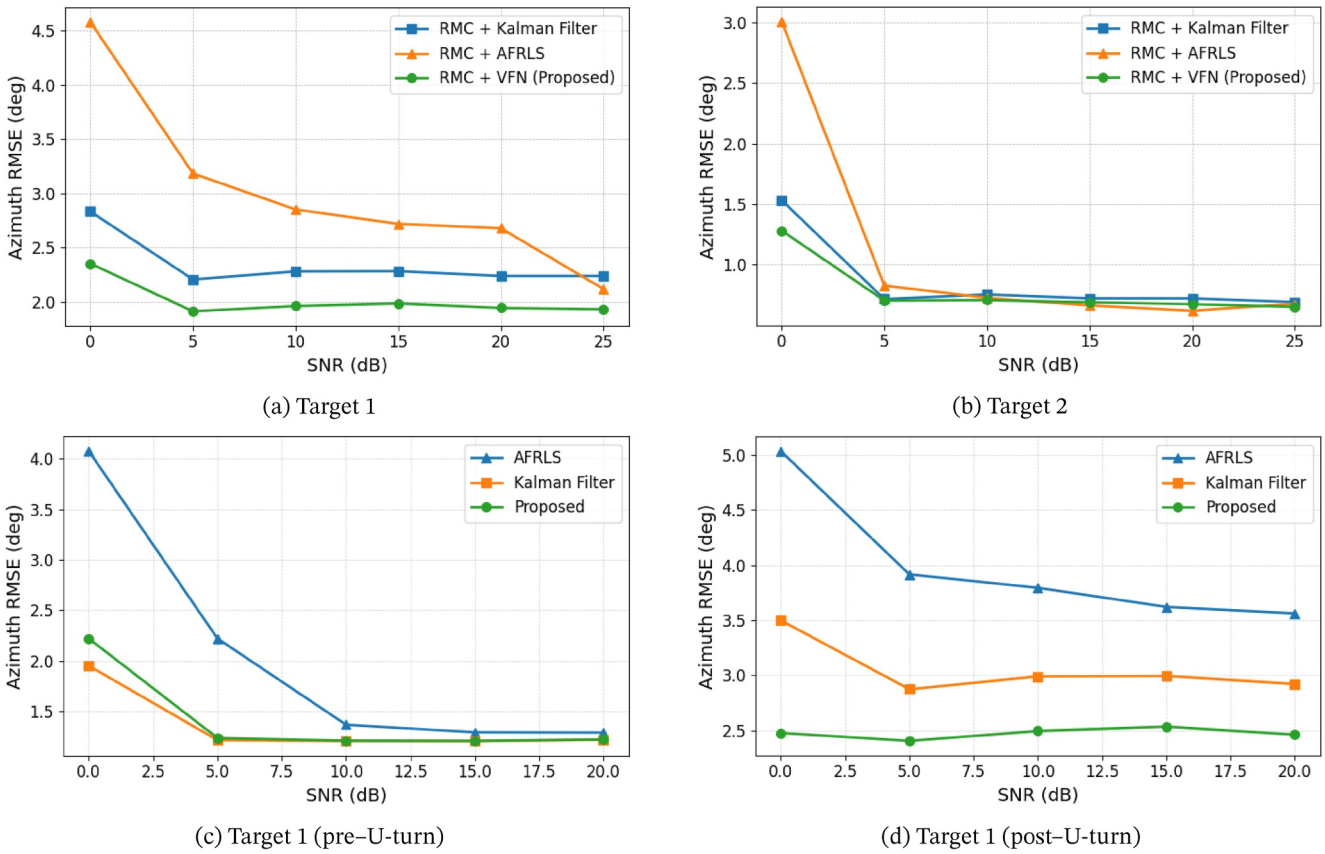


(a) Target 1

(b) Target 2

(c) Target 1 (pre–U-turn)

(d) Target 1 (post–U-turn)

**FIGURE 5** | Azimuth RMSE performance comparison of different tracking methods under varying SNR conditions. (a) Target 1. (b) Target 2. (c) Target 1 (pre–U-turn). (d) Target 1 (post–U-turn).

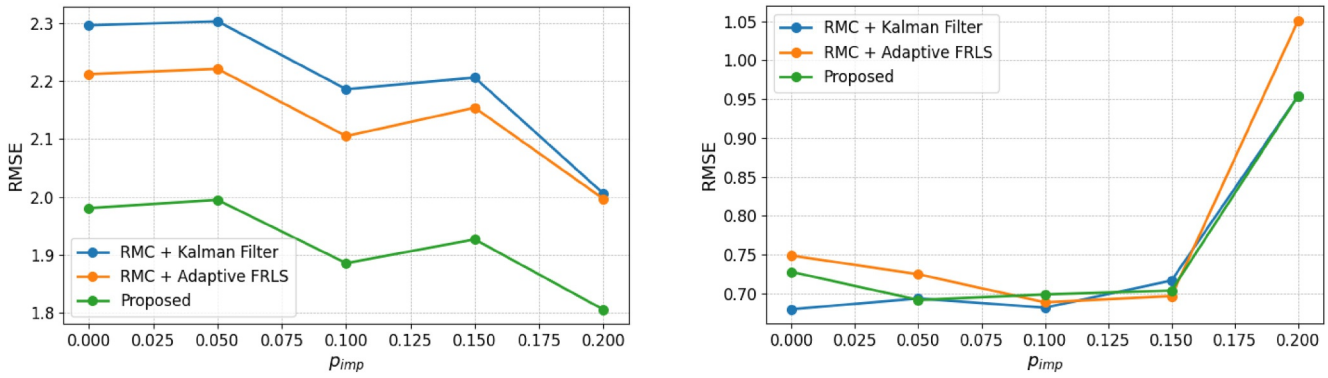


(a) Target 1 (b) Target 2

**FIGURE 6** | Azimuth RMSE performance versus impulsive noise probability $p_{\text{imp}}$. (a) Target 1. (b) Target 2.

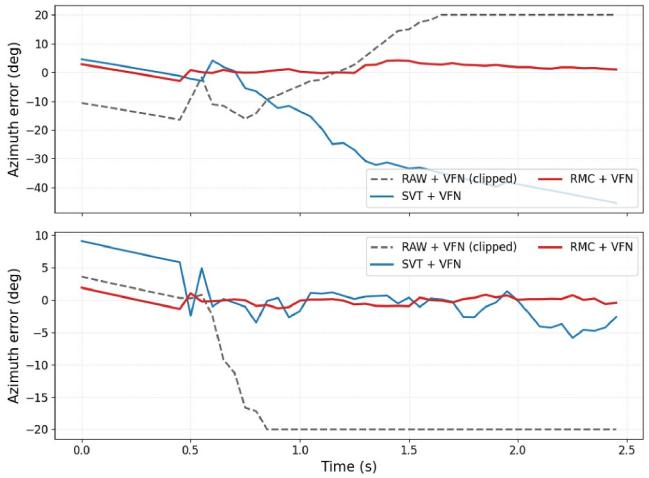


**FIGURE 7** | Azimuth tracking error versus time. The top and bottom subplots correspond to Target 1 and Target 2, respectively. The instantaneous absolute error is computed as $|\theta_{\text{est}} - \theta_{\text{true}}|$.

accumulates significant error, SVT + VFN shows moderate performance with residual fluctuations and the RMC-based tracker achieves the lowest instantaneous error with smooth convergence. These results confirm that robust matrix completion as a preprocessing stage is the dominant factor enabling stable azimuth tracking, with the specific choice of RMC-based tracker having negligible influence on instantaneous error.

## 4.1 | Ablation Study of the Proposed Pipeline

To quantify the contribution of each module, Table 2 compares beamspace-only estimation, tracking-only processing, partial RMC-based variants and the full proposed method, averaged over 50 Monte Carlo runs. The results demonstrate that tracking without robust covariance stabilisation is insufficient under sparse RIS observations. Subspace regularisation emerges as the dominant contributor, reducing the 2D RMSE by more than an order of magnitude relative to the beamspace-only and tracking-only baselines, whereas adaptive tracking provides consistent additional refinement. The full proposed method achieves the lowest overall 2D RMSE, confirming that robust low-rank regularisation and adaptive tracking yield complementary gains

**TABLE 2** | Ablation study.

| Method | Az RMSE | El RMSE | 2D RMSE |
|---|---|---|---|
| Beamspace only | 22.215 | 19.508 | 29.731 |
| Tracking only | 49.335 | 43.078 | 69.864 |
| RMC + beamspace | 3.456 | 2.444 | 4.347 |
| RMC + tracking (fixed) | 1.594 | 0.806 | 1.820 |
| RMC + tracking (var., no Huber) | 1.676 | 1.239 | 2.127 |
| **Proposed** | **1.482** | **0.866** | **1.750** |

*Note:* Bold values are referred to as proposed method results, representing the best results by highlighting them in bold.

and that reliable measurement recovery is a prerequisite for effective temporal tracking.

Table 3 presents an order-wise computational complexity analysis of the proposed framework relative to representative baselines. The framework comprises three stages: (i) beamspace-based DoA estimation, (ii) adaptive VFN-RLS tracking and (iii) robust low-rank preprocessing for sparse RIS measurements. Complexity is quantified in terms of complex multiplications per sensing epoch. The objective is to characterise the relative computational burden of each component rather than to establish strict real-time guarantees.

## 4.2 | Computational Complexity Analysis

### *4.2.1* | *Beamspace DoA Estimation*

The beamspace spatial spectrum is computed as

$$P(\phi, \theta) = \mathbf{a}^H(\phi, \theta)\hat{\mathbf{R}}(t)\mathbf{a}(\phi, \theta), \tag{39}$$

where $\hat{\mathbf{R}}(t) \in \mathbb{C}^{B\times B}$ is the beamspace covariance matrix and $\mathbf{a}(\phi, \theta) \in \mathbb{C}^{B\times 1}$ is the steering vector. For each grid point $(\phi, \theta)$, the dominant cost is a matrix-vector multiplication of complexity $\mathcal{O}(B^2)$. Evaluating the spectrum over a grid of $G = |\Phi| \times |\Theta|$ points thus yields a total complexity of unlike classical subspace methods such as MUSIC, the proposed approach requires no eigenvalue decomposition, significantly reducing the overall computational burden.

$$\mathcal{O}(GB^2). \tag{40}$$

#### 4.2.2 | *VFN-RLS Tracking*

The tracking stage operates on low-dimensional state and measurement vectors. For each target, the dominant operations—state prediction, covariance update, gain computation and state correction—involve matrices of dimension $d \times d$ and $m \times d$, yielding a per-target complexity of $\mathcal{O}(d^2)$, identical to that of conventional RLS-based trackers. The variable forgetting and noise adaptation mechanisms introduce only scalar operations and do not alter this complexity order.

#### 4.2.3 | *Robust Low-Rank Preprocessing*

The robust low-rank regularisation stage, implemented via Huber-loss ADMM, performs iterative singular value thresholding on an $M \times L$ data matrix. Retaining the leading $r$ singular values, the dominant cost per iteration scales as $\mathcal{O}(MLr)$. Since this stage is invoked selectively to stabilise covariance estimation under sparse or impulsive conditions rather than at every tracking step, it does not dominate the overall computational cost of the framework.

### 4.3 | Convergence Behaviour of ADMM Under Sparse Observations

To evaluate the computational behaviour of the robust low-rank regularisation stage, we analyse the convergence of the Huber-ADMM algorithm under varying sparsity levels. The RIS observation ratio is varied from 5% to 50% and the number of iterations required to satisfy the stopping criterion of Algorithm 2 is recorded across multiple realisations at each sparsity level.

Figure 8 illustrates the average number of ADMM iterations required for convergence as a function of the observed RIS element ratio. It can be seen that the algorithm consistently converges within approximately 7–9 iterations across all sparsity levels. Moreover, the error bars indicate very low variability across different realisations, demonstrating stable convergence behaviour even under highly sparse observations.

**TABLE 3** | Computational complexity comparison.

| Processing stage | Method | Complexity order |
|---|---|---|
| DoA estimation | MUSIC | $O(M^3 + GM^2)$ |
| DoA estimation | Proposed beamspace spectrum | $O(GB^2)$ |
| Tracking | Kalman filter (KF) | $O(d^3)$ |
| Tracking | AF-RLS | $O(d^2)$ |
| Tracking | Proposed VFN-RLS | $O(d^2)$ |
| Preprocessing | SVT-based matrix completion | $O(N_{\text{iter}}MLr)$ |
| Preprocessing | Proposed RMC (Huber-ADMM) | $O(N_{\text{iter}}MLr)$ |

Figure 9 shows the convergence success rate of the ADMM algorithm under varying sparsity levels. The results indicate that the proposed method achieves a 100% convergence rate across all tested observation ratios, confirming the reliability of the optimisation process. Overall, these results demonstrate that the proposed ADMM-based formulation exhibits stable and efficient convergence behaviour even under highly sparse RIS observations. This robustness is attributed to the low-rank structure of the signal model and the use of Huber loss, which mitigates the effect of impulsive disturbances.

### 4.4 | Impact of Impulsive Noise and Adaptive Tracking Behaviour

To investigate the interplay between subspace regularisation and adaptive forgetting, Figure 10 presents the 2D RMSE as a function of impulsive noise probability $p_{\text{imp}}$. Without subspace regularisation (RAW case), both fixed and adaptive forgetting trackers exhibit pronounced performance degradation with increasing $p_{\text{imp}}$. The adaptive variant is particularly susceptible, as it reacts strongly to corrupted DoA measurements, resulting in large and unstable tracking errors. Incorporating robust matrix completion (RMC) effectively stabilises the measurement space and maintains consistently low RMSE across all noise levels, confirming the importance of subspace regularisation in suppressing non-Gaussian disturbances. When further combined with adaptive forgetting, the proposed method achieves stable tracking without amplifying impulsive noise; the adaptive

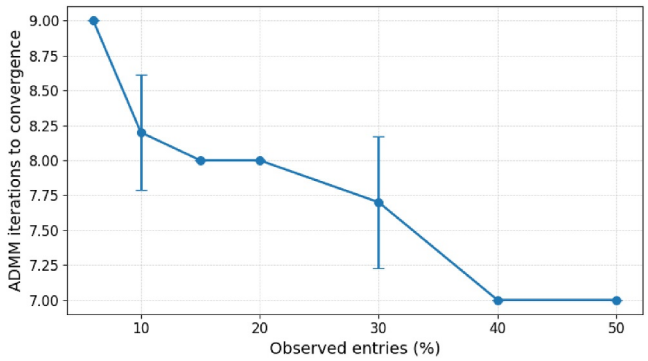


**FIGURE 8** | ADMM convergence iterations versus observed RIS element ratio.

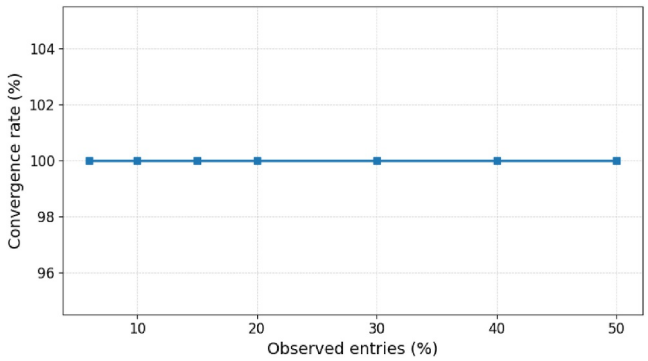


**FIGURE 9** | ADMM convergence success rate versus observed RIS element ratio.

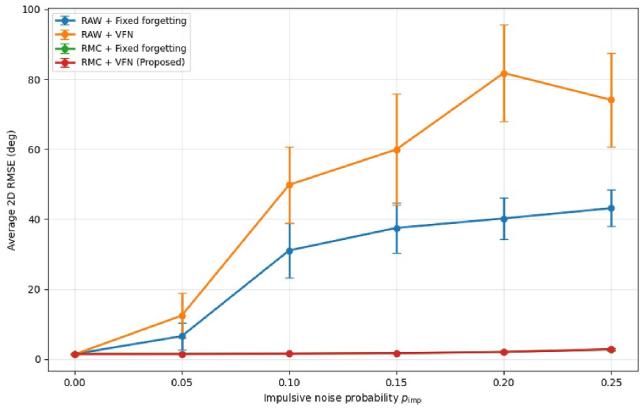


**FIGURE 10** | 2D RMSE versus impulsive noise probability $p_{\text{imp}}$.

mechanism provides controlled responsiveness to dynamic variations whilst preserving robustness. These results demonstrate that RMC and adaptive forgetting play complementary roles: the former ensures reliable measurement quality, whereas the latter enables flexible adaptation under nonstationary conditions.

## 5 | Conclusion

This paper presented a robust 2D DoA estimation and adaptive tracking framework for two moving vehicles in RIS-assisted vehicular sensing under sparse spatial observations. By combining beamspace-based DoA extraction with a variable-forgetting and noise-adaptive RLS tracker and low-rank regularisation preprocessing, the proposed approach achieves reliable angle tracking with only 6% of RIS elements activated per sensing slot. Simulation results confirmed accurate tracking of a challenging U-turn manoeuvre alongside a straight-trajectory vehicle, outperforming beamspace-only, tracking-only and partial-ablation baselines whilst remaining competitive with Kalman and AF-RLS trackers. These results validate the feasibility of low-complexity RIS-assisted sensing for intelligent transportation systems. Future work will target denser traffic settings, advanced target association and experimental validation in realistic environments.

### Author Contributions

**Farheen Naaz:** conceptualisation, formal analysis, investigation, methodology, validation, writing – original draft, writing – review and editing. **Sung Won Kim:** funding acquisition, supervision, writing – original draft.

### Acknowledgements

This research was supported by Basic Science Research Program through the National Research Foundation of Korea (NRF) funded by the Ministry of Education (RS-2021-NR060120), by the BK21 FOUR of the National Research Foundation of Korea (NRF) funded by the Ministry of Education (2120251015517), and by the NRF grant funded by the Korea government (MSIT) (RS-2022-NR069161).

### Conflicts of Interest

The authors declare no conflicts of interest.

### Data Availability Statement

Data available on request due to privacy/ethical restrictions.

### References

1. F. Liu, Y. Cui, C. Masouros, et al., "Integrated Sensing and Communications: Toward Dual-Functional Wireless Networks for 6G and Beyond," *IEEE Journal on Selected Areas in Communications* 40, no. 6 (2022): 1728–1767, https://doi.org/10.1109/jsac.2022.3156632.

2. J. A. Zhang, F. Liu, C. Masouros, et al., "An Overview of Signal Processing Techniques for Joint Communication and Radar Sensing," *IEEE Journal of Selected Topics in Signal Processing* 15, no. 6 (2021): 1295–1315, https://doi.org/10.1109/jstsp.2021.3113120.

3. Le Zheng, M. Lops, Y. C. Eldar, and X. Wang, "Radar and Communication Coexistence: An Overview: A Review of Recent Methods," *IEEE Signal Processing Magazine* 36, no. 5 (2019): 85–99, https://doi.org/10.1109/msp.2019.2907329.

4. A. R. Chiriyath, B. Paul, and D. W. Bliss, "Radar-Communications Convergence: Coexistence, Cooperation, and Co-Design," *IEEE Transactions on Cognitive Communications and Networking* 3, no. 1 (2017): 1–12, https://doi.org/10.1109/tccn.2017.2666266.

5. X. Cheng, D. Duan, S. Gao, and L. Yang, "Integrated Sensing and Communications (ISAC) for Vehicular Communication Networks (VCN)," *IEEE Internet of Things Journal* 9, no. 23 (2022): 23441–23451, https://doi.org/10.1109/jiot.2022.3191386.

6. P. Mollahosseini, R. Shen, T. A. Khan, and Y. Ghasempour, "Integrated Sensing and Communication: Research Advances and Industry Outlook," *IEEE Journal of Selected Topics in Electromagnetics, Antennas and Propagation* 1, no. 1 (2025): 375–392, https://doi.org/10.1109/jsteap.2025.3604368.

7. F. Liu and C. Masouros, "A Tutorial on Joint Radar and Communication Transmission for Vehicular Networks—Part I: Background and Fundamentals," *IEEE Communications Letters* 25, no. 2 (2021): 322–326, https://doi.org/10.1109/lcomm.2020.3025310.

8. Z. Feng, Z. Fang, Z. Wei, Xu Chen, Z. Quan, and D. Ji, "Joint Radar and Communication: A Survey," *China Communications* 17, no. 1 (2020): 1–27, https://doi.org/10.23919/jcc.2020.01.001.

9. Z. Du, F. Liu, Y. Li, et al., "Toward ISAC-Empowered Vehicular Networks: Framework, Advances, and Opportunities," *IEEE Wireless Communications* 32, no. 2 (2025): 222–229, https://doi.org/10.1109/mwc.002.2300496.

10. Z. Du, F. Liu, W. Yuan, et al., "Integrated Sensing and Communications for V2I Networks: Dynamic Predictive Beamforming for Extended Vehicle Targets," *IEEE Transactions on Wireless Communications* 22, no. 6 (2023): 3612–3627, https://doi.org/10.1109/twc.2022.3219890.

11. E. Basar, M. Di Renzo, J. De Rosny, M. Debbah, M.-S. Alouini, and R. Zhang, "Wireless Communications Through Reconfigurable Intelligent Surfaces," *IEEE Access* 7 (2019): 116753–116773, https://doi.org/10.1109/access.2019.2935192.

12. Q. Wu and R. Zhang, "Towards Smart and Reconfigurable Environment: Intelligent Reflecting Surface Aided Wireless Network," *IEEE Communications Magazine* 58, no. 1 (2020): 106–112, https://doi.org/10.1109/mcom.001.1900107.

13. M. Di Renzo, A. Zappone, M. Debbah, et al., "Smart Radio Environments Empowered by Reconfigurable Intelligent Surfaces: How It Works, State of Research, and the Road Ahead," *IEEE Journal on Selected Areas in Communications* 38, no. 11 (2020): 2450–2525, https://doi.org/10.1109/jsac.2020.3007211.

14. J. Zhang, E. Björnson, M. Matthaiou, D. W. K. Ng, H. Yang, and D. J. Love, "Prospective Multiple Antenna Technologies for Beyond 5G,"

*IEEE Journal on Selected Areas in Communications* 38, no. 8 (2020): 1637–1660, https://doi.org/10.1109/jsac.2020.3000826.

15. F. Naaz, A. Nauman, T. Khurshaid, and S.-W. Kim, "Empowering the Vehicular Network With RIS Technology: A State-of-the-Art Review," *Sensors* 24, no. 2 (2024): 337, https://doi.org/10.3390/s24020337.

16. A. Bazzi and M. Chafii, "Robust Integrated Sensing and Communication Beamforming for Dual-Functional Radar and Communications: Method and Insights," *arXiv preprint arXiv:2303.07652* (2023), https://doi.org/10.48550/arXiv.2303.07652.

17. A. Bazzi, D. T. M. Slock, and L. Meilhac, "Online Angle of Arrival Estimation in the Presence of Mutual Coupling," in *2016 IEEE Statistical Signal Processing Workshop (SSP)* (IEEE, 2016), 1–4.

18. D. Wang, A. Bazzi, and M. Chafii, "RIS-Enabled Integrated Sensing and Communication for 6G Systems," in *2024 IEEE Wireless Communications and Networking Conference (WCNC)* (IEEE, 2024), 1–6.

19. A. Bazzi and M. Chafii, "Low Dynamic Range for RIS-Aided Bistatic Integrated Sensing and Communication," *IEEE Journal on Selected Areas in Communications* 43, no. 3 (2025): 912–927, https://doi.org/10.1109/jsac.2025.3531533.

20. Q. Li, R. Li, K. Ji, and W. Dai, "Kalman Filter and Its Application," in *2015 8th International Conference on Intelligent Networks and Intelligent Systems (ICINIS)* (IEEE, 2015), 74–77.

21. M. I. Ribeiro, "Kalman and Extended Kalman Filters: Concept, Derivation and Properties," *Institute for Systems and Robotics* 43, no. 46 (2004): 3736–3741, https://d1wqtxts1xzle7.cloudfront.net/81315221/kalman-libre.pdf?1645663509=&response-content-disposition=inline%3B+filename%3DKalman_and_Extended_Kalman_Filters_Conce.pdf&Expires=1779512065&Signature=Xk3QuQLvYCd~bwQbdDhIm5XtFZr6VIW0iZiKLxN9ig9L3dUwMOVZl2k.

22. E. A. Wan and R. Van Der Merwe, "The Unscented Kalman Filter," in *Kalman Filtering and Neural Networks* (2001), 221–280.

23. C. Paleologu, J. Benesty, and S. Ciochina, "A Robust Variable Forgetting Factor Recursive Least-Squares Algorithm for System Identification," *IEEE Signal Processing Letters* 15 (2008): 597–600, https://doi.org/10.1109/lsp.2008.2001559.

24. L. Shan, H. Chen, J. Luan, and Li Jun, "Application of Adaptive Forgetting Factor RLS Algorithm in Target Tracking," in *2017 Chinese Automation Congress (CAC)* (IEEE, 2017), 1838–1843.

25. Y. Fang, S. Zhu, B. Liao, X. Li, and G. Liao, "Target Localization With Bistatic MIMO and FDA-MIMO Dual-Mode Radar," *IEEE Transactions on Aerospace and Electronic Systems* 60, no. 1 (2024): 952–964, https://doi.org/10.1109/taes.2023.3333829.

26. J. Zhang, Y. Ni, J. Li, et al., "Decision Transformers for RIS-Assisted Systems With Diffusion Model-Based Channel Acquisition," *arXiv preprint arXiv:2501.08007* (2026), https://doi.org/10.48550/arXiv.2501.08007.

27. J. Hu, H. Zhang, B. Di, et al., "Reconfigurable Intelligent Surface Based RF Sensing: Design, Optimization, and Implementation," *IEEE Journal on Selected Areas in Communications* 38, no. 11 (2020): 2700–2716, https://doi.org/10.1109/jsac.2020.3007041.

28. J. An, C. Xu, Lu Gan, and L. Hanzo, "Low-Complexity Channel Estimation and Passive Beamforming for RIS-Assisted MIMO Systems Relying on Discrete Phase Shifts," *IEEE Transactions on Communications* 70, no. 2 (2022): 1245–1260, https://doi.org/10.1109/tcomm.2021.3127924.

29. C. Lu, *A Library of ADMM for Sparse and Low-Rank Optimization* (National University of Singapore, 2016), https://github.com/canyilu/LibADMM.

30. C. Lu, J. Feng, S. Yan, and Z. Lin, "A Unified Alternating Direction Method of Multipliers by Majorization Minimization," *IEEE Transactions on Pattern Analysis and Machine Intelligence* 40, no. 3 (2018): 527–541, https://doi.org/10.1109/tpami.2017.2689021.

31. A. Jaiswal, Y. Wang, L. Yin, et al., "From Low Rank Gradient Subspace Stabilization to Low-Rank Weights: Observations, Theories, and Applications," in *Proceedings of the 42nd International Conference on Machine Learning* (PMLR, 2025).

32. A. Ertug Zorkun, M. A. Salas-Natera, R. M. Rodríguez-Osorio, and S. Chatzinotas, "Energy Efficient Low-Complexity RIS-Aided 3-D DoA Estimation and Target Tracking Algorithm via Matrix Completion," *IEEE Access* 12 (2024): 197929–197941, https://doi.org/10.1109/access.2024.3511717.

33. K. Li, J. Xiao, J.F. Xie, and R. Q. Wu, "A Novel Adaptive Variable Forgetting Factor RLS Algorithm," in *2022 International Conference on Informatics, Networking and Computing (ICINC)* (IEEE, 2022), 228–232.

34. E. Candes and B. Recht, "Exact Matrix Completion via Convex Optimization," *Communications of the ACM* 55, no. 6 (2012): 111–119, https://doi.org/10.1145/2184319.2184343.

35. P. J. Huber, *Robust Estimation of a Location Parameter* (Springer New York, 1992), 492–518.

36. S. Boyd, N. Parikh, E. Chu, B. Peleato, and J. Eckstein, "Distributed Optimization and Statistical Learning via the Alternating Direction Method of Multipliers," *Foundations and Trends in Machine Learning* 3, no. 1 (2011): 1–122, https://doi.org/10.1561/2200000016.

37. J.-F. Cai, E. J. Candes, and Z. Shen, "A Singular Value Thresholding Algorithm for Matrix Completion," *SIAM Journal on Optimization* 20, no. 4 (2010): 1956–1982, https://doi.org/10.1137/080738970.